Tunable Dual-Wavelength Fiber Laser in a Novel High Entropy van der Waals Material

Wen-Wen Cui(崔文文), Xiao-Wei Xing(邢笑伟), Yue-Qian Chen(陈悦芊), Yue-Jia Xiao(肖悦嘉), Han Ye(叶寒), and Wen-Jun Liu(刘文军)*

State Key Laboratory of Information Photonics and Optical Communications, School of Science, Beijing University of Posts and Telecommunications, Beijing 100876, China

(Received 22 December 2022; accepted manuscript online 17 January 2023)

Fiber lasers with different net dispersion cavity values can produce some types of solitons, and rich nonlinear dynamics phenomena can be achieved by selecting different saturable absorbers. A new layered high-entropy van der Waals material (HEX) (Mn,Fe,Co,Ni)PS_3 was selected as a saturable absorber to achieve a high-power laser output of 34 mW. In addition, the wavelength can be dynamically tuned from 1560 nm to 1531 nm with significant dual-wavelength phenomena at 460 fs pulse duration.

DOI: 10.1088/0256-307X/40/2/024201

Passive mode-locked fiber lasers can generate stable ultrashort pulses by building cavity structures with different net dispersions,[1] including conventional solitons,[2] dissipative solitons,[3] dispersion-managed solitons,[4] self-similar solitons,[5] and many other forms of mode-locked laser. In the process of achieving passive mode-locking, the nonlinear dynamics between solitons can be revealed by balancing intracavity dispersion and nonlinearity,[6–9] thus explaining the evolution of laser mode-locking, including phenomena such as soliton molecules,[10] soliton pulsation,[11] soliton explosion,[12] soliton rain,[13] dissipative soliton resonance,[14] rogue waves,[15] bound state solitons,[16] harmonic mode-locking,[17] and dual-wavelength mode locking.[18] The characteristics of different soliton evolution processes are used to guide the development in aerospace, military, communications,[19] and other fields. For example, dual-wavelength mode locking is widely used in dual-comb spectroscopy,[20–22] high-resolution spectroscopy, and laser ranging. In addition, multi-wavelength mode locking can also be divided into synchronous and asynchronous pulse lasers due to different pulse speeds at different wavelengths. Synchronous pulse lasers[23] can be used in the terahertz field,[24] and asynchronous pulse lasers[25] can be used in pump-probe technology.

In fiber lasers based on passive mode-locking technology, saturable absorbers[26–32] are the key to achieving mode-locking self-initiation. As a new type of two-dimensional layer structure material, a high-entropy van der Waals material (HEX)[33] can achieve flexible modulation of physical properties such as energy band structure and spin intensity[34,35] because of its weaker interlayer interaction forces,[36] which allows it to be used for making spintronic devices[37] while also satisfying the modulation effect of saturable absorbers on lasers.

In this Letter, a dynamically tunable dual-wavelength mode-locked fiber laser in a negative-dispersion cavity is realized by precisely managing the full-cavity dispersion value and selecting a new high-entropy van der Waals material (Mn,Fe,Co,Ni)PS_3 as a saturable absorber. Mode-locked pulses of 460 fs at 1531 nm and 487 fs at 1557 nm were obtained. The full process of dynamic switching of dual-wavelength solitons in different polarization states is observed experimentally, and the high-power narrow-pulse-width dual-wavelength mode-locking phenomenon is achieved in the communication window band. The results show that (Mn,Fe,Co,Ni)PS_3 in the high-entropy van der Waals material has excellent optoelectronic properties with large modulation depth for pulse narrowing, which can also be useful for observing soliton nonlinear dynamics phenomena to some extent.

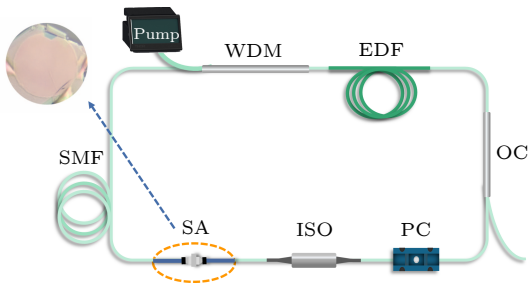

Fig. 1. Optical path structure of an all-fiber mode-locked fiber laser.

Figure 1 shows an all-fiber laser resonant cavity based on (Mn,Fe,Co,Ni)PS_3. The resonant cavity consists of a 976 nm pump source, a wavelength division multiplexer (WDM) with a specification of 980/1550 nm, a 1.5 m erbium-doped fiber (EDF) with an absorption coefficient of 30 dB/m, and a dispersion parameter D of −12.5 ps/(km·nm), and a section of a 13.2 m single-mode fiber (SMF) with a dispersion parameter of 18 ps/(km·nm), and saturable absorbers. The total length of the resonant cavity is 14.7 m and the net dispersion of the full cavity is $-0.272\,\mathrm{ps}^2$. The unidirectional transmission of the optical pulses is ensured by the ISO and the modulation of

*Corresponding author. Email: jungliu@bupt.edu.cn
© 2023 Chinese Physical Society and IOP Publishing Ltd

the polarization state of the optical pulses is achieved by adjusting the access PC. A 90 : 10 fiber optic coupler was used to output optical pulses, and the output pulse signal was detected by a high-speed oscilloscope (SDS6204 H12 Pro) with a sampling rate of 10 GSa/s, and a 2 GHz bandwidth, a spectrum analyzer (Yokogawa AQ6370B), a spectrum analyzer (Agilent E4402B), and an autocorrelator (APE Pulse check).

The modulation depth of high entropy alloy (Mn,Fe,Co,Ni)PS_3 is 28.5%, which can be used as a saturable absorber in the laser. The detection device and modulation depth curve are shown in Fig. 2. The dual-arm balanced detection device in Fig. 2 is composed of a laser pulse source, an attenuator, a 50 : 50 optical fiber coupler, and a power meter. The mode-locked pulse light is divided into two channels after passing through the attenuator and being coupled by the optical fiber coupler. Among them, one channel of the probe light is directly measured as a power reference, and the other channel of the probe light passes through the material, thus reflecting the absorption of the material under different light intensities. The attenuator is used to adjust the laser intensity. A 50 : 50 optical circulator (OC) was taken to ensure that the two channels of light could be evenly divided.

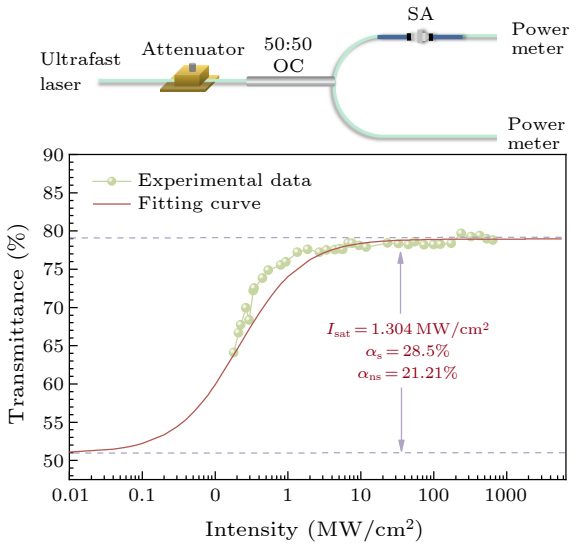

Fig. 2. Detection device and modulation depth curve.

Based on the measured data, we can fit the modulation depth curve of the (Mn,Fe,Co,Ni)PS_3 material. The modulation model reads

$$\alpha(I) = \frac{\alpha_s}{1 + I/I_{sat}} + \alpha_{ns}, \tag{1}$$

where α_s is the saturation loss representing the modulation depth, α_{ns} is the unsaturated loss, I_{sat} is the saturation strength, and the fitted modulation depth curve is shown in Fig. 2.

The laser achieves stable self-starting mode locking when the pump power exceeds the mode-locking threshold. The number of pulses is gradually reduced as the pumping power is continuously reduced, eventually achieving a single pulse output. When the pump power is 187 mW, there is continuous wave operation at about 1560 nm. After fine-tuning the polarization controller (PC), the output spectrum has a typical Kelly sideband, which is characteristic of the traditional soliton mode locking spectrum in the negative dispersion region. The central wavelength of the spectrum is 1557 nm, with the 3 dB bandwidth being 9.8156 nm, as shown in Fig. 3.

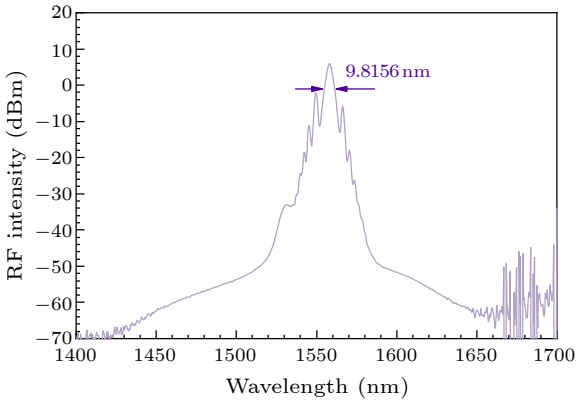

Fig. 3. Conventional soliton spectrum at 1560 nm.

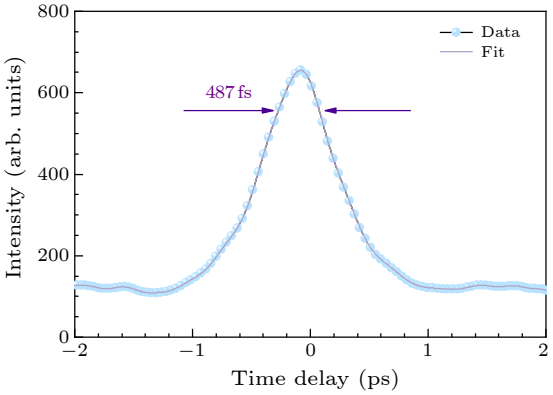

Fig. 4. Autocorrelation curve after 487 fs pulse duration fitting.

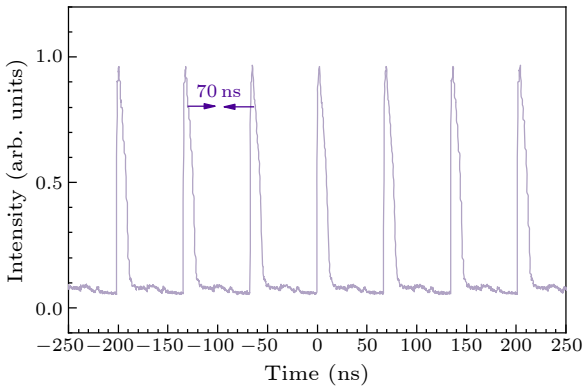

Fig. 5. Oscilloscope output pulse sequence at 1560 nm.

The autocorrelation curve was fitted using the sech^2 function, as shown in Fig. 4, with a pulse duration of 487 fs and a time-bandwidth product (TBP) calculated to be 0.47, indicating a slight chirp in the output conventional soliton. Figure 5 shows a sequence diagram of the oscilloscope output pulses, from which it can be seen that the output sequence has equal pulse intensities and the spacing between adjacent pulses corresponds to a cavity cycle of

approximately 70 ns. The sequence diagram of the pulses provides further evidence that there is only one soliton pulse in the resonant cavity at this time. The laser mode-locking threshold is 83.57 mW and the maximum output power at the full pump is 33.85 mW. The measurement results of the spectrum are shown in Fig. 6, showing that the fundamental frequency of the pulse is 14.8896 MHz and the signal-to-noise ratio is 74.92 dB, proving that the laser can operate stably in the mode-locked state.

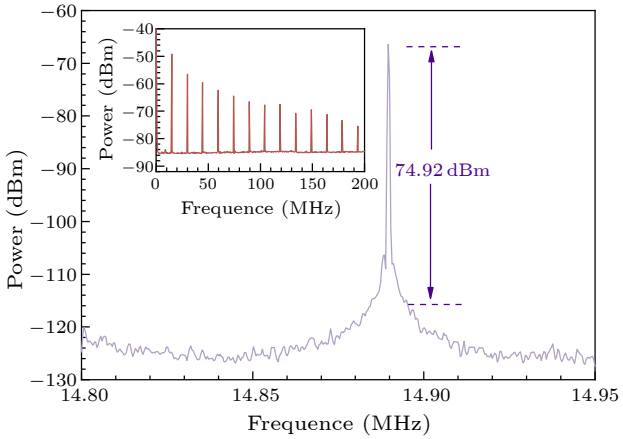

Fig. 6. Measured pulse spectrum of the laser at 1560 nm.

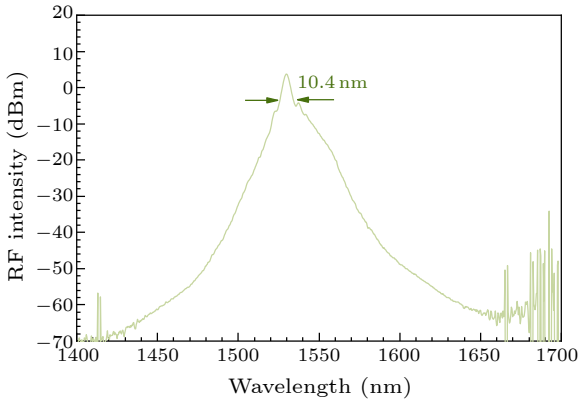

Fig. 7. Conventional soliton spectrum at 1531 nm.

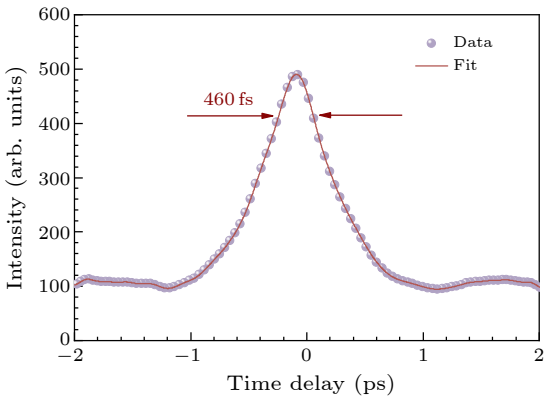

Fig. 8. Autocorrelation curve after 460 fs pulse duration fitting.

As the pump power is increased to 271 mW and the PC is rotated, the polarization state of the optical pulse in the cavity changes, and a continuous wave near 1530 nm can be observed from the OSA, with the micro-spin PC achieving a complete offset of the mode-locked wavelength. At this time, restarting the pump can still automatically start mode locking at 1530 nm. At this time, the observation of the OSA spectrum shows that the central wavelength is 1531 nm, and the 3 dB bandwidth is 10.4 nm, as shown in Fig. 7. The pulse duration curve is shown in Fig. 8, with a pulse duration of 460 fs, corresponding to a TBP of 0.47, indicating a slight chirp in the output conventional soliton. The output pulse sequence is shown in Fig. 9, with a pulse cycle period of approximately 70 ns. The laser mode-locking threshold is 71.36 mW and the maximum output power at the full pump is 34.33 mW. With a repetition frequency of 14.8897 MHz and a signal-to-noise ratio of 67.59 dBm, the spectrum plotted in Fig. 10 proves that the laser can achieve stable mode locking.

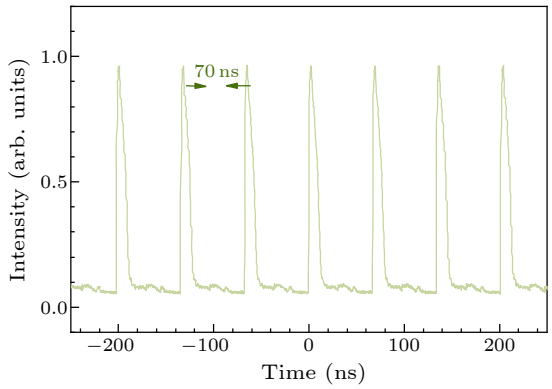

Fig. 9. Output pulse sequence from oscilloscope at 1531 nm.

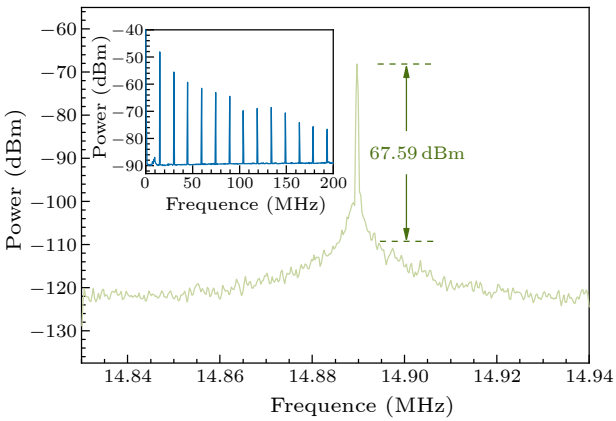

Fig. 10. Measured pulse spectrum of the laser at 1531 nm.

By slowly adjusting the polarization state, the full process of dynamic switching of the dual-wavelength mode-locking can be seen. Figure 11 shows the spectral plots of the solitons at the two dual wavelengths and the spectral features of the coexistence of the two wavelength solitons in the intermediate switching process. The central wavelengths and bandwidths of both wavelengths are consistent with the previous results. Figure 12 shows the oscilloscope

traces, and the trajectory of the two pulse movements can be seen in the sequence diagram. By adjusting the oscilloscope trigger, you can see the phenomenon of one pulse being stationary and the other moving periodically.

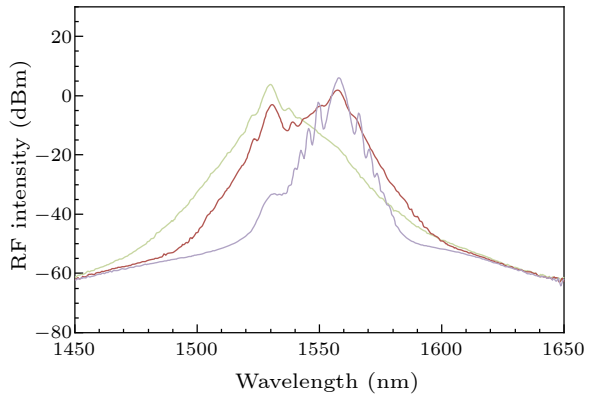

Fig. 11. Diagram of the dynamic switching process of dual-wavelength solitons.

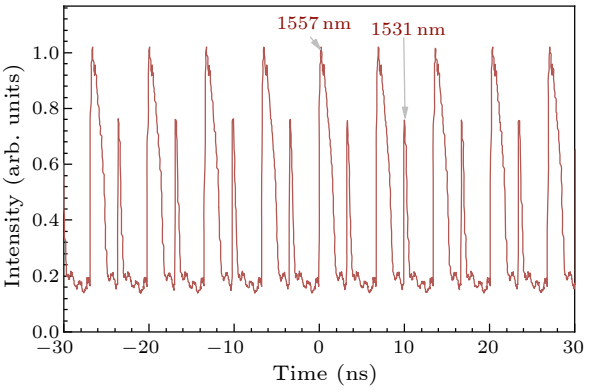

Fig. 12. Two-wavelength soliton sequence diagram.

The prerequisite for being able to achieve dual wavelength mode locking with different wavelengths is to have similar gain coefficients. Birefringence in the optical cavity is regulated by inserting (Mn,Fe,Co,Ni)PS_3 in the optical cavity and adjusting the polarization controller to produce the dual-wavelength mode locking phenomenon. The phenomenon of soliton mode locking of the laser at 1531 nm and 1560 nm can be seen in Fig. 11. As the pulse undergoes periodic gain and loss in the laser, to maintain the soliton characteristics, the pulse emits some of its energy as a dispersive wave, forming a spectral sideband.

In conclusion, we have proved that (Mn, Fe,Co, Ni)PS_3 not only is a high-performance photocatalyst, but also can be used to increase the pulse output power up to 34 mW, narrow the pulse duration to 460 fs in fiber lasers, realize the dual-wavelength mode-locking phenomenon in the negative net dispersion cavity in the communication window band, and achieve dynamic tunability of wavelengths from 1560 nm to 1531 nm. In future research, high-entropy alloys can also be applied to net dispersive cavities with different dispersion values to realize richer nonlinear dynamical phenomena such as bound state solitons, multi-wavelength mode locking, and soliton pulsation to further explain microscopic dynamic phenomena of laser mode locking.

References

[1] Keller U 2003 *Nature* **424** 831
[2] Cui Y D and Liu X M 2013 *Opt. Express* **21** 18969
[3] Grelu P and Akhmediev N 2012 *Nat. Photon.* **6** 84
[4] Turitsyn S K, Bale B G, and Fedoruk M P 2012 *Phys. Rep.* **521** 135
[5] Oktem B, Ülgüdür C, and Ö I F 2010 *Nat. Photon.* **4** 307
[6] Porsezian K, Hasegawa A, Serkin V N, Belyaeva T L, and Ganapathy R 2007 *Phys. Lett.* **361** 504
[7] Ganapathy R 2012 *Commun. Nonlinear Sci.* **17** 4544
[8] Ma G L, Zhao J B, Zhou Q, Biswas A, and Liu W J 2021 *Nonlinear Dyn.* **106** 2479
[9] Liu W J, Shi T, Liu M L, Wang Q, Liu X M, Zhou Q, Lei M, Lu P F, and Wei Z Y 2021 *Opt. Express* **29** 29402
[10] Peng J S and Zeng H P 2018 *Laser Photon. Rev.* **12** 1800009
[11] Liu M, Wei Z W, Li H, Li T J, Luo A P, Xu W C, and Luo Z C 2020 *Laser Photon. Rev.* **14** 1900317
[12] Peng J S and Zeng H P 2019 *Phys. Rev. Appl.* **12** 034052
[13] Chouli S and Grelu P 2010 *Phys. Rev. A* **81** 063829
[14] Chang W, Ankiewicz A, Soto-Crespo J M, and Akhmediev N 2008 *Phys. Rev. A* **78** 023830
[15] Song Y F, Wang Z H, Wang C, Panajotov K, and Zhang H 2020 *Adv. Photon.* **2** 024001
[16] Li K X, Song Y R, Tian J R, Guoyu H Y, and Xu R Q 2017 *IEEE Photon. J.* **9** 1400209
[17] Liu X M and Pang M 2019 *Laser Photon. Rev.* **13** 1800333
[18] Yan Z, Li X, Tang Y, Shum P P, Yu X, Zhang Y, and Wang Q J 2015 *Opt. Express* **23** 4369
[19] Wang X Z, Wang Z H, Wang Y Y, Zhang X, Song J J, and Wei Z Y 2021 *Chin. Phys. Lett.* **38** 074202
[20] Ni X, Jia K, Wang X, Liu H, Guo J, Huang S W, and Zhu S N 2021 *Chin. Phys. Lett.* **38** 064201
[21] Zhang J, Hua L Q, Chen Z, Zhu M F, Gong C, and Liu X J 2020 *Chin. Phys. Lett.* **37** 124203
[22] Ning K, Hou L, Fan S T, Yan L L, Zhang Y Y, Rao B J, and Jiang H F 2020 *Chin. Phys. Lett.* **37** 064202
[23] Stojanovic N and Drescher M 2013 *J. Phys. B* **46** 192001
[24] Guan Z, Wang G L, Zhang L, Jiao Z H, Zhao S F, and Zhou X X 2021 *Chin. Phys. Lett.* **38** 054201
[25] Zhao X, Zheng Z, Liu L, Wang Q, Chen H, and Liu J 2012 *Opt. Express* **20** 25584
[26] Liu W, Liu M, Liu X, Wang X, Teng H, Lei M, and Wei Z 2020 *Appl. Phys. Lett.* **116** 061901
[27] Liu W, Xiong X, Liu M, Xing X, Chen H, Ye H, and Wei Z 2022 *Appl. Phys. Lett.* **120** 053108
[28] Liu M, Wu H, Liu X, Wang Y, Lei M, Liu W, and Wei Z 2021 *Opto-Electron. Adv.* **4** 200029
[29] Nizamani B, Salam S, Jafry A A A, Zahir N M, Jurami N, Khudus M A, and Harun S W 2020 *Chin. Phys. Lett.* **37** 054202
[30] Liu J T, Yang F, Lu J P, Ye S, Guo H W, Nie H K, Zhang J L, He J L, Zhang B T, and Ni Z H 2022 *Nat. Commun.* **13** 3855
[31] Yang S, Zheng J C, Qi Y Y, Shi Y W, Li D, Nie X C, and Sun Z P 2023 *Opt. Laser Technol.* **157** 108726
[32] Poddubrovskii N R, Lobach I A, and Kablukov S I 2022 *Opt. Laser Technol.* **156** 108568
[33] Ying T, Yu T, Shiah Y S, Li C, Li J, Qi Y, and Hosono H 2021 *J. Am. Chem. Soc.* **143** 7042
[34] Gong C and Zhang X 2019 *Science* **363** eaav4450
[35] Manzeli S, Ovchinnikov D, Pasquier D, Yazyev O V, and Kis A 2017 *Nat. Rev. Mater.* **2** 17033
[36] Molle A, Goldberger J, Houssa M, Xu Y, Zhang S C, and Akinwande D 2017 *Nat. Mater.* **16** 163
[37] Li J, Yang X, Liu Y, Huang B, Wu R, Zhang Z, and Duan X 2020 *Nature* **579** 368